Exploring the benefits beyond the pre-reduction in methane of the Cr/SiO2 Phillips catalyst: The molecular structure of the Cr sites and their role in the catalytic performance

Exploring the benefits beyond the pre-reduction in methane of the Cr/SiO_2 Phillips catalyst: The molecular structure of the Cr sites and their role in the catalytic performance

CaterinaBarzan[a] AlessandroPiovano[a] MariaBotavina[a] Giorgia A.Martino[a] GiovanniAgostini[b] GianmarioMartra[a] ElenaGroppo[a]

[a] Department of Chemistry, NIS Centre and INSTM, University of Torino, via P. Giuria 7, 10125 Torino, Italy

[b] ERSF – European Synchrotron Radiation Facility, 71 Avenue des Martyrs, 38000 Grenoble, France

Abstract

A pre-reduction of the Cr^{VI}/SiO_2 Phillips catalyst in methane at 400 °C eliminates the induction time in ethylene polymerization and enhances the catalyst activity of ca. 30%, despite maintaining the polymer properties almost unaltered. By coupling together several spectroscopic techniques (FT-IR, DR UV-Vis-NIR and XANES spectroscopies, coupled with mass spectrometry) we have been able to identify and quantify the reduced Cr sites present in the catalyst after the pre-reduction treatment and to detect some of the reaction by-products. In particular, formic acid and hydrogen are released during the pre-reduction. The presence of hydrogen in the reaction mixture justifies the formation of ca. 33% of 6-fold coordinated Cr^{III} sites, which however do not take part to the catalysis being fully coordinated. In addition, ca. 23% of the Cr^{VI} sites are converted into highly uncoordinated Cr^{II} sites, while the remaining 44% are reduced to Cr^{IV}(=O) sites. Although both Cr^{II} and Cr^{IV}(=O) are accessible by incoming molecules, most of the credits for the improved catalytic activity go to Cr^{IV}(=O), which have been already demonstrated to be one order of magnitude more active than Cr^{II}.

Graphical abstract

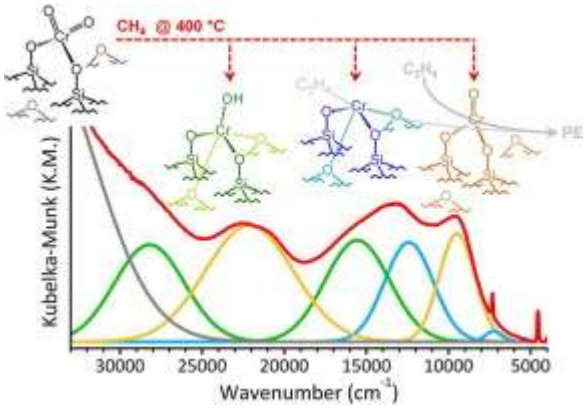

1. Introduction

In the polyolefin market, polyethylene (PE) accounts for more than 160 billions of dollars per year, rising approximately four percent every year [1]. The majority of PE, whose economic success relies in the low cost, versatility and recyclability [2], is produced in a catalytic way. Therefore, in the years to come any improvement of ethylene polymerization catalysts in terms of performances, customization and yield will become crucial to keep on riding the polyolefin market [3], [4], [5]. To this aim, identifying which are the reasons behind serendipitous discoveries of high-performing systems is the basis for the *ad hoc* design of new catalysts or modification of the existing ones [6], [7], [8], [9], [10].

Among ethylene polymerization catalysts, the Cr-based Phillips catalysts contribute to more than 50% of the High Density Polyethylene (HDPE) market [11], [12], [13]. It is generally constituted by monochromates [14], [15], [16], [17], [18], [19] highly dispersed on amorphous silica [20], which are slowly converted into the active sites in the presence of ethylene at 80–110 °C during the so called “induction period” [21], [22], [23], [24]. Hence, ethylene serves as activating agent (with the double function of reducing and alkylating the Cr sites) and also as the monomer in the polymerization reaction. What happens into the reactor during the induction time has been debated for long time, and still constitutes one of the major arguments of discussion. Recently, some of us provided compelling evidence for the reduction of monochromates to Cr^{II} species and oxygenated by-products (mainly methylformate), that remain in strong interaction with the Cr^{II} sites also during the initial steps of ethylene polymerization [23]. This is in very good agreement with previous findings by McDaniel and co-workers, who demonstrated that under commercial ethylene polymerization conditions oxygenates may remain attached to the chromium sites [25]. At the same time, a small fraction of Cr^{III} sites are also formed, mainly as a consequence of the reduction of the Cr^{V} species unavoidably present in the oxidized catalyst [26], [27]. We

also demonstrated that the hindered Cr^{II} sites are key intermediates involved in ethylene polymerization, while it is not clear whether or not the Cr^{III} species have a role in the same reaction [26], [27]. According to these results, ethylene works as a two-electron reducing agent during the induction time.

In the industrial practice other reducing agents are often used before (or even during) the introduction of ethylene into the polymerization reactor. Their use is aimed at diminishing or completely eliminating the induction period and to conduct the ethylene polymerization at lower temperature (e.g. as demanded to produce UHMWPE) [10], [15], [28], [29], [30], [31], [32], [33], [34], [35], [36], [37]. The most efficient and cleanest reducing agent is carbon monoxide, which stoichiometrically reduces the monochromates at 350 °C to give highly uncoordinated Cr^{II} species and volatile CO_2 through a two-step two-electron pathway [38], [39], [40], [41]. These divalent chromium species were deeply characterized [18], [27], [42] and they are nowadays uncontrovertibly considered as the intermediates involved in ethylene polymerization on the CO-reduced Cr/SiO_2 Phillips catalyst [26], [41], [43]. The highly uncoordinated Cr^{II} sites obtained through CO reduction readily react with O_2 to give a brilliant light flash of luminescence [11], [44]. Despite the cleanness of the CO reduction procedure, CO is at present scarcely used by polyolefin companies, mainly because of its toxicity. Other pre-reducing agents commonly adopted in the industrial practice are H_2, alkanes (e.g. hexane), alkenes (e.g. cyclohexene) and metal alkyls (such as AlR_3, BR_3, MgR_2, ZnR_2) [11], [13]. With the exception of metal alkyls, which are effective already at room temperature, most of the other reducing agents operate at higher temperature (being the preferred temperature range around 350–400 °C) and give a pre-reduced catalyst that reacts with air giving the luminescent flash characteristic of highly uncoordinated Cr^{II} sites [11], [13].

Besides affecting the induction time, the pre-reduction procedure influences the polymer properties and in particular the amount of *in situ* branching, that means the polymer density. Generally all the mentioned agents have an influence. For example, according to Max McDaniel, pre-reduction in CO at 350 °C produces a polymer with a density of ca. 0.928 g mL^{-1}, compared to that of ca. 0.959 g mL^{-1} obtained starting from the traditional Cr^{VI}/SiO_2 catalyst (in both cases at 95 °C in the presence of 5 ppm of BEt_3 co-catalyst) [11], [13]. This means that the pre-reduction procedure affords reduced Cr sites at least partially different from those obtained upon direct reduction in ethylene. Such a difference might be traced to the absence of the oxygenated by-products nearby the Cr^{II} sites in the catalysts pre-reduced at a temperature higher than the polymerization temperature [27]. However, this is not sufficient to explain why different reducing

agents operating at a similar temperature give different polymers. In this context, we turned our attention on the effects of methane. According to McDaniel, a Cr^{VI}/SiO_2 catalyst pre-reduced in methane at 400 °C produces under the same reaction conditions described above a PE with a density of ca. 0.947 g mL^{-1} (i.e. a slightly greater tendency to *in situ* branching) and, more interestingly, exhibits an activity ca. 30% higher than the unmodified Cr^{VI}/SiO_2 [11]. These observations implicate the presence of reduced Cr sites with a peculiar local structure. This work is devoted to their investigation, carried out using complementary spectroscopic methods, namely FT-IR, diffuse reflectance (DR) UV-Vis-NIR and X-ray absorption near edge structure (XANES) spectroscopies, applied *in situ* in the presence of gas molecules.

2. Experimental

2.1. Catalyst synthesis and activation procedures

The Cr/SiO_2 catalysts employed for the DR UV-Vis-NIR and FT-IR experiments were prepared by wet-impregnation at room temperature of SiO_2 (Aerosil®380, surface area ca. 380 $m^2\ g^{-1}$) with an aqueous solution of CrO_3, as described elsewhere [18], [42], [45]. Two batches of Cr/SiO_2 were synthesized, with a chromium loading of 0.5 wt% (for DR UV–Vis-NIR measurements) and 1.0 wt% (for FT-IR measurements). The choice was done to optimize the spectral quality. The XANES measurements were performed on a 2 wt% Cr/SiO_2 sample prepared by direct hydrothermal synthesis, as described elsewhere [46], [47], [48]. Briefly, a gel of SiO_2 and chromium nitrate (pH = 11) was heated in autoclave at 100 °C in the presence of cetyltrimethylammonium bromide as the structure-directing agent, then the so obtained powder was filtered, washed, heated into a gas-flow furnace at 600 °C under N_2 flux and finally calcined in O_2 at the same temperature. This sample was selected to allow collecting fast XANES spectra (12 min per spectrum) of reasonable quality (need to increase the Cr content) at the same time avoiding Cr aggregation during the thermal treatments (an unavoidable phenomenon for Cr/SiO_2 catalysts obtained by wet-impregnation at Cr loadings above 1 wt%). Cross-checking experiments demonstrated that the spectroscopic properties of the three samples are the same irrespective of the Cr loading [18]. For this reason, in the following we will not distinguish the three samples in terms of synthesis procedure and Cr content, but only in terms of activation treatment and oxidation state. Throughout the text we will use always the nomenclature Cr^n/SiO_2, where the n indicates the oxidation state (when known).

All the samples were subjected to the same thermal treatments, either in static (for FT-IR and DR UV–Vis-NIR measurements) or in flow (for XANES measurements) conditions. The catalyst activation was performed in the presence of O_2 at 650 °C, resulting in the oxidized catalyst deeply investigated in the past [18], [27], [42] and hereafter labeled as Cr^{VI}/SiO_2. The pre-reduction treatment was performed in methane at 400 °C, to give CH_4-Cr/SiO_2. For sake of reference, the pre-reduction of Cr^{VI}/SiO_2 was performed also in the presence of CO at 350 °C, to give the well-known Cr^{II}/SiO_2 [18], [27], [42]. A second reference sample was prepared by treating Cr^{II}/SiO_2 in the presence of N_2O at 100 °C, followed by degassing at the same temperature. According to our previous work [34], this treatment selectively converts most of the Cr^{II} sites into chromyl species, $Cr^{IV}(=O)$. This reference sample will be referred to as $Cr^{IV}(=O)/SiO_2$.

When working in static conditions (FT-IR and DR UV–Vis-NIR measurements), the reactive gases (equilibrium pressure 200 mbar) were dosed twice on the sample at the reaction temperature, followed by outgassing under dynamic vacuum at the same temperature to remove all the volatile by-products. FT-IR and DR UV–Vis-NIR spectra were collected at room temperature at the end of each step. When working in flow conditions, the reactive gases were fluxed at 40 mL/min through the measurement cell at atmospheric pressure. The investigation of the pre-reduction step was accomplished by continuously monitoring the XANES spectra at constant time interval in two different conditions: (1) flowing CH_4 directly at 400 °C; or (2) flowing CH_4 at increasing temperature from 50 to 400 °C. The final result was the same in the two cases. Only the sequence of XANES spectra collected at constant temperature will be shown for simplicity. However, the experiment performed at increasing temperature allowed determining the temperature of onset for reduction and also a better appreciation of some by-products by means of on-line MS.

Finally, ethylene polymerization was run on both CH_4-Cr/SiO_2 and Cr^{II}/SiO_2. The reaction was performed in static conditions in the gas phase, admitting 100 mbar of C_2H_4 on the catalyst at room temperature (25 °C), and continuously monitoring the FT-IR spectra of the catalyst during the reaction. The relative polymerization rate was determined by analyzing the intensity of the $\delta(CH_2)$ IR absorption band at 1472 cm^{-1}, once that the spectra were normalized to the optical thickness of the pellet (evaluated from the intensity of the overtones of SiO_2 framework in the 2000–1500 cm^{-1} range) [34].

2.2. Techniques

FT-IR spectroscopy. FT-IR spectra were collected with a Bruker Vertex70 instrument equipped with a MCT detector, at a resolution of 2 cm^{-1}. The samples were measured in the form of thin self-supporting pellets (surface density ca. 20 mg cm^{-2}) within a quartz cell with two KBr windows, suitable for thermal treatments and measurements in the presence of gases. For CO adsorption at room temperature, an equilibrium pressure P_{CO} of 50 mbar was sent on the sample, and a FT-IR spectrum was collected. Successively, the P_{CO} was gradually decreased followed by step-by-step collection of the FT-IR spectra. For the spectra in the presence of C_2H_4, see above.

Diffuse Reflectance UV–Vis-NIR spectroscopy. DR UV–Vis-NIR spectra were collected in diffuse reflectance mode with a Varian Cary5000 spectrophotometer, equipped for reflectance measurements with an integrating sphere with the inner surface coated by Spectralon®. The samples were measured in the form of very thick pellets (ca. 200 mg/cm^2 of surface density) within a cell with a window in Suprasil optical quartz. All the spectra were collected in reflectance and successively converted into Kubelka-Munk function.

XAS spectroscopy. X-ray absorption near edge structure (XANES) spectra at the Cr K-edge (5989 eV) were collected at the BM23 beamline [49] at the European Synchrotron Radiation Facility (ESRF, Grenoble, F). The white beam was monochromatized by a Si(1 1 1) double crystal. Harmonic rejection was performed by using silicon mirrors (4 mrad). The intensity of the incident beam was measured with an ionization chamber. The spectrum of the reference Cr_2O_3 (Sigma-Aldrich) was measured in transmission mode, whereas all the other XAS spectra were collected in fluorescence mode by means of a silicon drift detector. The catalyst was measured in the form of powder inside a quartz capillary (1.5 mm outer diameter and 10 μm of wall thickness), placed in between two small regions of quartz wool. The capillary was connected to a gas-dosing system with mass-flow controllers, and inserted inside an oven equipped with a temperature controller. The reaction products were qualitatively detected with a mass spectrometer placed at the end of the capillary. XANES spectra were acquired with an energy step of 0.4 eV and an integration time of 2 s per point, up to $k = 5$ $Å^{-1}$ in order to allow easy and reliable normalization. Each XANES spectrum required an acquisition time of about 12 min. The XANES spectra were normalized using the Athena program (from the Ifeffit program suite) [50]. The adopted experimental set-up (low Cr loading, fluorescence acquisition, capillary, quite small scattering volume) did not allow collection of EXAFS spectra with a satisfactory signal-to-noise ratio.

3. Results and discussion

3.1. Ethylene polymerization performances

At first, the ethylene polymerization rate of CH_4-Cr/SiO_2 was investigated in comparison to that of Cr^{II}/SiO_2, in order to assess if the macroscopic differences pointed out in industrial conditions [11], [13] can be detected also by a spectroscopic analysis at lab scale. Fig. 1 shows the *in situ* FT-IR spectra collected within the first two minutes of ethylene polymerization on Cr^{II}/SiO_2 (part a) and on CH_4-Cr/SiO_2 (part b), in both $\nu(CH_2)$ (left) and $\delta(CH_2)$ (right) regions. All the spectra are shown after subtraction of the spectrum of the catalyst before ethylene addition and normalization to the optical thickness of the pellet, to allow a quantitative comparison.

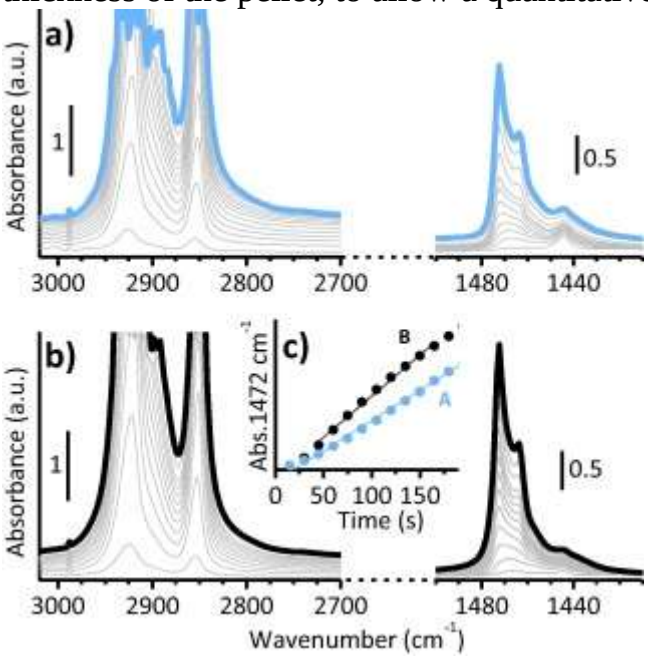

Fig. 1. Evolution of the FT-IR spectra collected during ethylene polymerization (PC_2H_4 = 100 mbar, T = 25 °C) on Cr^{II}/SiO_2 (part a) and on CH_4-Cr/SiO_2 (part b). The spectra are shown in the $\nu(CH_x)$ and $\delta(CH_x)$ spectral regions (from left to right) as a function of the polymerization time up to 3 min, after subtracting the spectra of the catalysts prior ethylene addition and normalizing to the optical thickness of the pellet (for sake of quantitative comparison). (Part c) evolution of the intensity of the 1472 cm^{-1} IR absorption band as a function of time for the ethylene polymerization on Cr^{II}/SiO_2 (A) and on CH_4-Cr/SiO_2 (B).

In both cases the FT-IR spectra show the immediate appearance and very fast increase in intensity of some absorption bands at 2920, 2855 and 1472 cm^{-1}, which are assigned to the asymmetric and symmetric stretching and bending vibrational modes of the CH_2 moieties in polyethylene [51], [52], [53]. This means that the CH_4-Cr/SiO_2 catalyst rapidly polymerizes ethylene without any induction time, at room temperature and low pressures, as also Cr^{II}/SiO_2 does. The reaction rate, evaluated from the time evolution of the intensity of the $\delta(CH_2)$ band at 1472 cm^{-1} (Fig. 1c), is ca. 27% higher for CH_4-

Cr/SiO_2, in very good agreement with the literature [11], [13]. This indicates either that the fraction of Cr active sites is higher, or that they are characterized by a different molecular structure, or both. To explore the reasons of such reactivity, we moved to the characterization of the CH_4-Cr/SiO_2 catalyst, by focusing the attention on the structural and electronic properties of the Cr sites and their environment with several spectroscopic techniques.

3.2. Evidence for Cr^{VI} reduction and possible by-products

Fig. 2a displays the FT-IR spectra of Cr^{VI}/SiO_2 and CH_4-Cr/SiO_2, in comparison to that of pure SiO_2 treated in O_2 at 650 °C. The spectrum of SiO_2 is characterized by a sharp absorption band at 3748 cm^{-1} due to the ν(OH) of surface isolated silanols, and by the off-scale signals due to the vibrational modes of the framework below 1280 cm^{-1}, also responsible for the characteristic pattern in the 2000–1500 cm^{-1} range, due to combination (1970 and 1865 cm^{-1}) and overtone (1640 cm^{-1}) modes [54]. The spectrum of Cr^{VI}/SiO_2 is that typical of a highly dehydroxylated silica, except for the characteristic band at 910 cm^{-1} (in the so called "transparency window" of silica), which is due to a perturbation of the SiO_2 vibrational modes induced by the presence of chromates, and for the weak band at 1980 cm^{-1} (magnified in the right inset), assigned to the first overtone of ν(Cr = O_2) [18], [55], [56]. Both bands are drastically affected by the pre-reduction treatment in CH_4, testifying an almost complete reduction of the chromates.

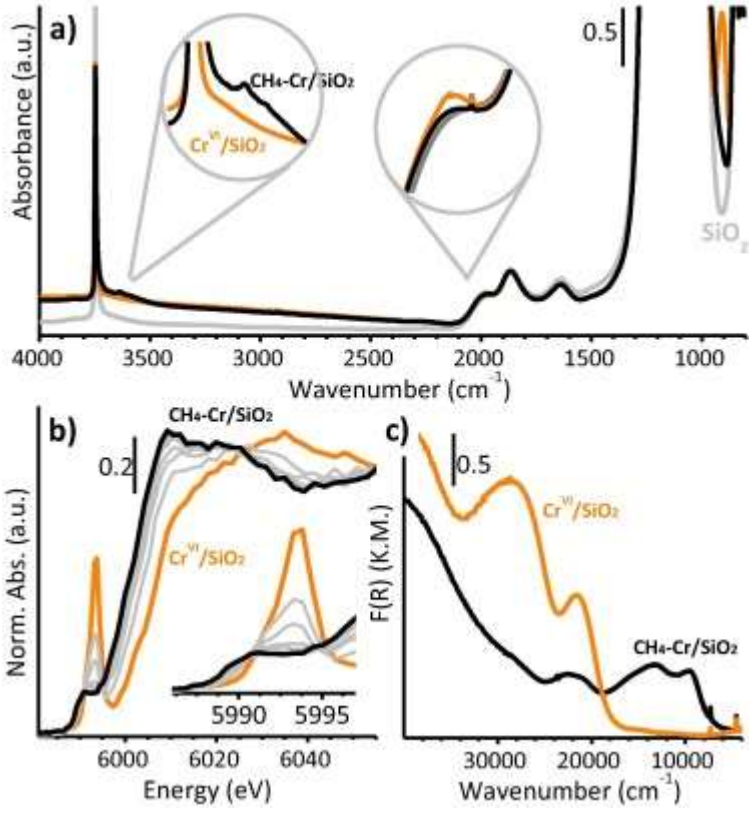

Fig. 2. FT-IR (part a), Cr K-edge XANES (part b) and DR UV–Vis-NIR (part c) spectra of Cr^{VI}/SiO_2 and CH_4-Cr/SiO_2. For XANES, also the intermediate spectra collected every 12 min in *operando* conditions are shown (grey spectra). In part a, the spectrum of pure silica (grey) is added for sake of comparison, and two relevant portion of the spectra are magnified in the insets.

No new bands are observed in the ν(CH_x) region, indicating that all the organic by-products deriving from CH_4 oxidation and hydrolysis leave the catalyst surface under the reaction conditions. The only exception is a broad IR absorption band in the ν(OH) region, detailed with two weak and narrow bands at 3637 and 3587 cm^{-1} (left inset in Fig. 1a). These bands do not seem correlated to a modification of the isolated silanols, neither are formed when treating pure silica in the same conditions (Figure S1). Therefore, they are tentatively ascribed to new hydroxy groups formed upon the reaction between CH_4 (or a by-product) with some Cr oxo-species (i.e., the chromates or their derivatives). Similar ν(OH) bands were observed in the past on α-chromia dehydroxylated under dynamic vacuum at 400 °C [57].

The reduction of almost all the chromates of Cr^{VI}/SiO_2 during the thermal treatment in CH_4 at 400 °C is corroborated by *operando* Cr K-edge XANES and *in situ* DR UV–Vis-NIR data (Fig. 2b and c, respectively). The XANES and DR UV–Vis-NIR spectra of Cr^{VI}/SiO_2 have been already discussed in the past [18], [27], [42], [48], [58], and are characteristic of highly diluted mono-chromate species. In particular, the XANES spectrum has the edge at 6007.6 eV and is dominated by an intense pre-edge peak at 5993.5 eV, which is indicative of a tetrahedral coordination [47], [59], [60], [61]. The DR UV–Vis-NIR spectrum is characterized by three absorption bands at ca. 39500, 29000 and 21500 cm^{-1}, which are due to O → Cr charge transfer transitions [14], [15], [17], [42]. As soon as Cr^{VI}/SiO_2 is contacted by CH_4 at 400 °C, the XANES and DR UV–Vis-NIR spectra rapidly change (spectra 1 in Fig. 2b and c). In the XANES the following changes are observed: (i) the edge (evaluated at the maximum of the derivative signal) shifts from 6006.7 to 6003.3 eV; (ii) the sharp pre-edge peak decreases in intensity and broadens, accounting at the end for a total intensity of about 0.16 (in normalized absorption units); and (iii) the white-line changes its shape, with a prominent feature appearing at 6009.9 eV. In the DR UV–Vis-NIR spectrum, a group of bands appear below 20000 cm^{-1} (maxima at 13300 and 9500 cm^{-1}), in the typical region of the d-d bands, at the expenses of the bands associated to the chromates.

A sequence of XANES spectra similar to those reported in Fig. 2b were collected by treating Cr^{VI}/SiO_2 in the presence of CH_4 at increasing temperature from 50 to 400 °C. This experiment (not shown) allowed determining the temperature onset for reducing Cr^{VI} in methane (ca. 330 °C), and also monitoring by on-line mass-spectroscopy some

by-products of the reaction, which are formic acid and hydrogen. Interestingly, these by-products are compatible with the stoichiometric reaction:$Cr^{VI}/SiO_2 + CH_4 \rightarrow Cr^{II}/SiO_2 + HCOOH + H_2$where the mono-chromates present in Cr^{VI}/SiO_2 are reduced to highly uncoordinated Cr^{II} sites, similar to those obtained by reducing Cr^{VI}/SiO_2 in CO at 350 °C. This is compatible with the observation of the chemiluminescent flash upon exposure of CH_4-Cr/SiO_2 to air, as reported by McDaniel [11], [13] and observed by ourselves. However, the situation is not so simple as it might appear. Indeed, neither the XANES nor the DR UV–Vis-NIR spectra of CH_4-Cr/SiO_2 are the same as Cr^{II}/SiO_2 (vide infra Fig. 3a and b), indicating that additional reduced Cr sites must be present besides the highly uncoordinated Cr^{II}.

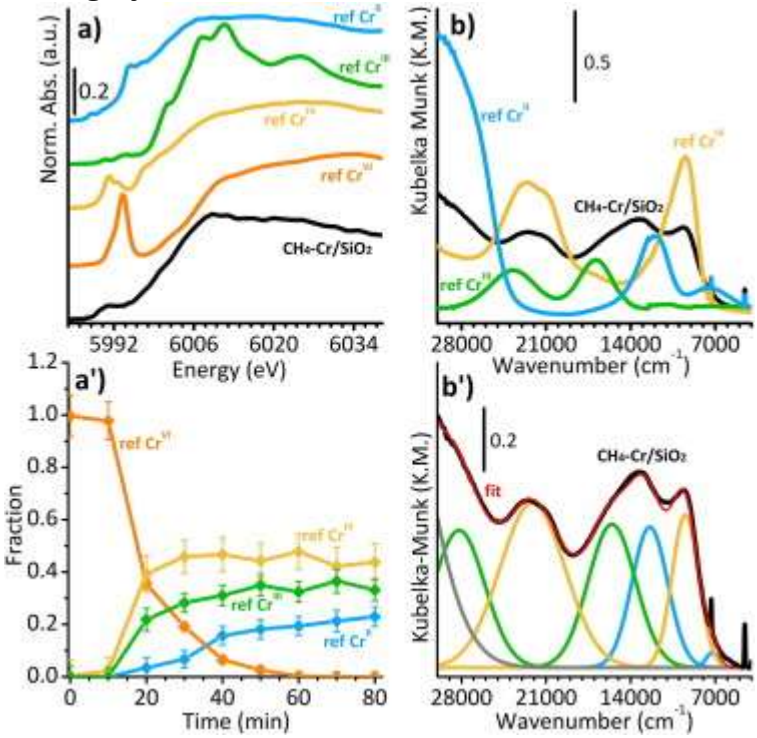

Fig. 3. Cr K-edge XANES (part a) and DR UV–Vis-NIR (part b) spectra of CH_4-Cr/SiO_2 compared to the spectra of some reference compounds with a well-defined Cr oxidation state; namely, Cr^{VI}/SiO_2 $Cr^{IV}(=O)/SiO_2$, Cr_2O_3, and highly uncoordinated Cr^{II}/SiO_2. (Part a′) Linear combination fit of the XANES spectra shown in Fig. 2b. (Part b′) Band fitting of the DR UV–Vis-NIR spectrum of CH_4-Cr/SiO_2: the experimental spectrum (black) is compared to the best fitting curve (red).

3.3. Evidence for the presence of multiple reduced Cr sites

The interpretation of both the XANES and DR UV-Vis-NIR spectra of CH_4-Cr/SiO_2 is complicated by the fact that the electronic features of the reduced Cr sites depend on both the oxidation state and the ligands sphere [27], [35], [62], and the two effects are difficult to be disentangled. A possible strategy to interpret the unknown spectra is to

compare them with those of selected reference compounds. This approach works incredibly well when the XANES and DR UV–Vis-NIR spectra are analyzed together. Fig. 3 shows the XANES (part a) and DR UV–Vis-NIR (part b) spectra of CH_4-Cr/SiO_2 compared to the following references: Cr^{II}/SiO_2, a Cr^{III} reference (either Cr_2O_3 or hexa-aquo $CrCl_3$, in parts a and b, respectively) and $Cr^{IV}(=O)/SiO_2$ [34], [63]. The XANES spectrum of Cr^{II}/SiO_2, whose edge is located at ca. 6000 eV, shows an intense and well resolved pre-edge peak at 5994 eV (assigned to a Cr1s → Cr4p transition) and two very weak pre-edge peaks at 5988 and 5990 eV (assigned to Cr1s → (Cr3d + O2p) dipole-forbidden transitions) [27], [42], [59], [61], [64]. The corresponding DR UV–Vis-NIR spectrum shows two narrow bands at ca. 12000 and 7500 cm^{-1}, having a relative intensity ratio of 5:1 [18], [27], [42]. As far as the Cr^{III} reference is concerned, the XANES spectrum of Cr_2O_3 exhibits the edge at 6002 eV, a very intense white-line, and two weak pre-edge peaks at 5990.5 and 5993.6 eV (assigned to the dipole-forbidden transitions of Cr^{III} species in an octahedral-like geometry) [48], [58]. The UV–Vis-NIR spectrum of a 6-fold coordinated Cr^{III} complex is generally characterized by a couple of bands at 24000 and 17000 cm^{-1}, having almost the same intensity [65], [66], [67]. Finally, the XANES spectrum of $Cr^{IV}(=O)/SiO_2$, whose edge is localized at 6004 eV, shows two distinct pre-edge peaks of medium intensity at 5991.2 and 5992.6 eV, with a shoulder on the edge around 5997.3 eV. The corresponding DR UV–Vis-NIR spectrum is characterized by two very intense bands at 22000 and 9500 cm^{-1}, the former quite broad, that are the typical d-d transition bands of 4-fold coordinated transition metals with a d^2 electronic configuration [34], [65], [68].

Both the XANES and the DR UV–Vis-NIR spectra of CH_4-Cr/SiO_2 contain the characteristic features of all the three references, suggesting that several types of reduced Cr sites are co-present. In order to quantify the relative fraction of each species, we fit the whole sequence of XANES spectra collected during the pre-reduction treatment (Fig. 2b) with a linear combination of the reference spectra [69]. The result of the LCF analysis are reported in Fig. 3a'. Almost 75% of the Cr^{VI} sites are reduced during the first 20 min of reaction, mainly in favor of $Cr^{IV}(=O)$ and 6-fold coordinated Cr^{III}. Uncoordinated Cr^{II} sites start to contribute to the XANES spectrum only at a later time and their fraction gradually increases likely at the expenses of the other reduced species (which indeed do not increase anymore, despite the Cr^{VI} reduction proceeds to completion). At the end of the reaction, Cr^{VI} does not contribute anymore to the XANES spectrum, while $Cr^{IV}(=O)$, 6-fold coordinated Cr^{III}, and uncoordinated Cr^{II} sites account for 44, 33 and 23%, respectively. The reliability of the LCF analysis is proved by the fact that the sum of all the contributions at each step is very close to 100% even without

imposing any mathematical constraints. The LCF analysis of the XANES spectra is validated by the qualitative analysis of the DR UV–Vis-NIR spectrum of CH_4-Cr/SiO_2 in the d-d spectral region. Indeed, the spectrum can be easily deconvolved into a number of components having positions and relative intensities in well agreement with those characteristic of the references, as reported in Fig. 3b′ (more details in Table S1a).

3.4. The reduced Cr sites: Accessibility and role in ethylene polymerization

In a successive step, we concentrated our attention on the accessibility of the diverse Cr sites in CH_4-Cr/SiO_2. To this aim, we employed FT-IR spectroscopy of adsorbed CO as a probe molecule [70], [71], [72]. Fig. 4a shows the FT-IR spectra of CO adsorbed on CH_4-Cr/SiO_2 at decreasing CO coverage (θ_{CO}) in the ν(C≡O) region.

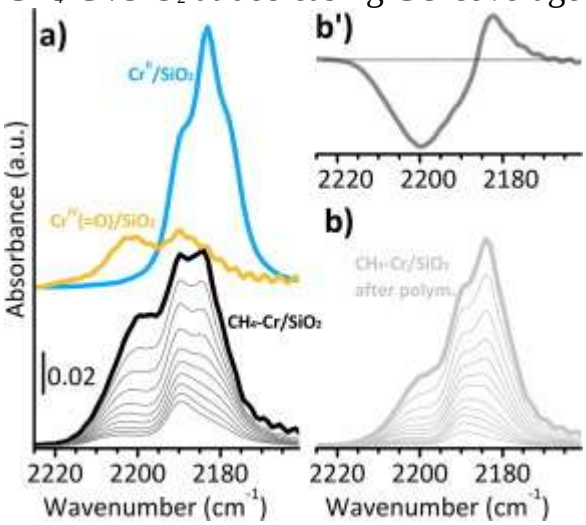

Fig. 4. (Part a) FT-IR spectra of CO adsorbed on CH_4-Cr/SiO_2 at decreasing θ_{CO} in the ν(C≡O) region. The spectra are reported after subtraction of that collected prior CO dosage. For comparison, also the spectra of CO adsorbed on the Cr^{II}/SiO_2 (blue) [18] and $Cr^{IV}(=O)/SiO_2$ (orange) [63], [73] references are reported, after normalization to the optical thickness of the pellets. (Part b) The same as part a) for CH_4-Cr/SiO_2 after 20 s of ethylene polymerization (P_{C2H4} = 50 mbar). (Part b′) Difference between the spectra of CO adsorbed on CH_4-Cr/SiO_2 before and after ethylene polymerization.

The spectrum at the maximum θ_{CO} is characterized by three main absorption bands at 2200, 2190 and 2184 cm^{-1}, with a pronounced shoulder at 2179 cm^{-1}. The latter three bands are the same as those observed for CO adsorbed on Cr^{II}/SiO_2 (spectrum also reported in Fig. 4a), and assigned to CO in interaction with two different families of Cr^{II} species characterized by a different number of coordination vacancies: on Cr^{II}_A two CO molecules are adsorbed at the maximum θ_{CO} (bands at 2184 and 2179 cm^{-1}) while on Cr^{II}_B only monocarbonyl adducts are formed (band at 2190 cm^{-1}) [18], [27], [39], [42], [74]. The band at 2200 cm^{-1} is assigned to CO in interaction with $Cr^{IV}(=O)$ sites. Indeed, a similar band was assigned to the same species

by Kohler and Ekerdt for Cr^{VI}/SiO_2 photo-reduced in CO [75], and successively by some of us for Cr^{II}/SiO_2 selectively oxidized by N_2O [63] or CO_2 [73]. For comparison, the spectrum of CO adsorbed on the $Cr^{IV}(=O)/SiO_2$ reference is also reported [63]. The evolution of the FT-IR spectra upon reducing θ_{CO} is in well agreement with this interpretation: indeed, the band at 2200 cm^{-1} decreases faster in intensity, indicating that CO is less strongly adsorbed on the $Cr^{IV}(=O)$ than it is on Cr^{II} sites. Hence, FT-IR spectroscopy of adsorbed CO indicates that both the highly uncoordinated Cr^{II} and the $Cr^{IV}(=O)$ sites are accessible to incoming molecules (including the monomer), while the 6-fold coordinated Cr^{III} sites are not.

In order to evaluate which are the sites involved in ethylene polymerization, the same experiment was repeated for CH_4-Cr/SiO_2 after 20 s of exposure to ethylene (Fig. 4b). The band at 2200 cm^{-1} is drastically decreased in comparison with the previous case at equal CO coverage (about 45% less), meaning that most of the $Cr^{IV}(=O)$ sites are no more available because they are occupied by the incipient polymer chains. In contrast, the three bands assigned to CO in interaction with Cr^{II} sites remain almost unaltered. This observation indicates that the Cr sites fastest to start ethylene polymerization are the $Cr^{IV}(=O)$ sites. However, this method cannot be applied for longer polymerization times [76], because the catalyst pellet is rapidly covered by a polymer layer that prevents CO diffusion.

For this reason, ethylene polymerization onto CH_4-Cr/SiO_2 was also monitored by DR UV–Vis-NIR spectroscopy, as showed in Fig. 5a. The formation of the polymer is indicated by the appearance of the typical fingerprints of PE in the NIR region, namely the overtones and combinations of the vibrational modes of CH_2 moieties (inset in Fig. 5a′). The overall absorbance is decreased because of the white polymer coating around the catalyst particles [77], [78], which changes their scattering properties [23]. However, a more careful glance clearly reveals that some bands are more affected than others, denoting which are the sites where the formation of the polymer takes place [79]. Fig. 5b reports the band fitting of the final spectrum (collected after 10 min of ethylene polymerization), showing an analogous composition as the one in Fig. 3b′, but with a different relative proportion of the contributions (the numerical data of the analysis are reported in Table S1). Although an absolute quantification of all the species cannot be achieved because it should require the knowledge of the extinction coefficients of all the absorption bands, we can estimate the relative variation of each species upon ethylene polymerization by comparing the relative intensities of the corresponding bands. For instance, if we assume the Cr^{III} sites as a benchmarks (since they were demonstrated to be almost inaccessible to incoming molecules), the ratio between the Cr^{IV} and

Cr^{III} integrated areas decreases by 63% (from 1.064 to 0.395), and that between the Cr^{II} and Cr^{III} by 38.5% (from 0.377 to 0.232). This means that at longer polymerization times most of the Cr^{IV}(=O) sites are involved (much more than those responsible for the first stages of reaction), followed by a considerable fraction of Cr^{II} sites. Such analysis cannot exclude that some Cr^{III} sites are active, but their amount is negligible in proportion and thus they cannot account for the overall great activity of the CH_4-Cr/SiO_2 catalyst.

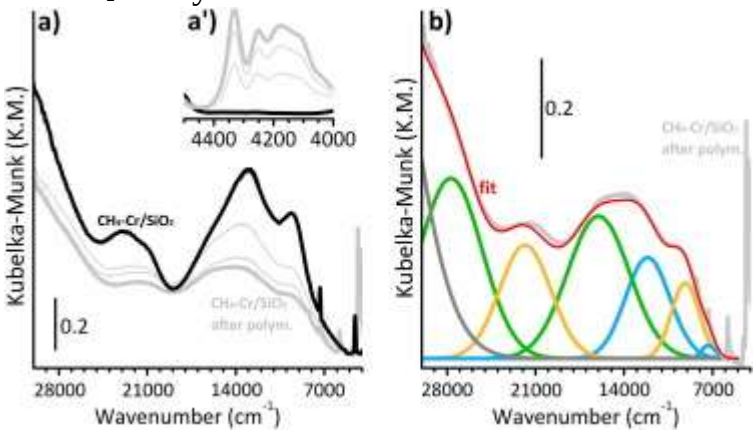

Fig. 5. (Part a) Evolution of the DR UV–Vis-NIR spectra of CH_4-Cr/SiO_2 during ethylene polymerization (for a total reaction time of 10 min). The inset in part a′ shows a magnification of the NIR region. (Part b) Band fitting of the DR UV–Vis-NIR spectrum of CH_4-Cr/SiO_2 after 10 min of ethylene polymerization: the experimental spectrum (light grey) is compared to the best fitting curve (red).

Therefore, FT-IR and DR UV–Vis-NIR spectroscopies converge in identifying the Cr^{IV}(=O) species as the main actors in the catalytic polymerization of ethylene on CH_4-Cr/SiO_2. This fully explains the great performances reported in the literature for a Cr^{VI}/SiO_2 catalyst pre-reduced in methane [11]. In fact, according to our previous work [34], the Cr^{IV}(=O) species are one order of magnitude more active than the highly uncoordinated Cr^{II} sites, and probably also of the more shielded Cr^{II} sites derived from ethylene reduction.

4. Conclusions

In this work, several spectroscopic techniques have been applied in a concerted way to unravel the effects of pre-reducing the Cr^{VI}/SiO_2 Phillips catalyst in CH_4 at 400 °C. According to industrial reports [11], [13], this procedure removes the induction time and enhances the catalyst activity of ca. 30%, at the same time maintaining the polymer properties almost unaltered. The economic advantages of this pre-reduction procedure are evident. Hence, it is of crucial importance understanding the effects that a pre-reduction in CH_4 has on the molecular structure of the chromium sites.

The results here shown clearly demonstrate that, in contrast with the most famous (though infrequently used in commercial processes) pre-reduction treatment in CO that cleanly converts all the Cr^{VI} sites to highly uncoordinated Cr^{II}, upon reduction by methane at least three types of reduced Cr species are formed, differing in the oxidation state (Cr^{II}, Cr^{III} and Cr^{IV}) and coordination geometry (as roughly depicted in Fig. 6). Formic acid and hydrogen have been detected as by-products of methane oxidation, and they are completely removed from the catalyst surface under the pre-reduction conditions. The relative amount of the three types of sites has been quantitatively determined by analyzing the XANES data. At the end of the pre-reduction treatment, about 33% of the Cr^{VI} sites are converted into 6-fold coordinated Cr^{III} sites (Fig. 6b), which are evidently not accessible to incoming molecules. Hence, their role in ethylene polymerization should be negligible. In addition, ca. 23% of the Cr^{VI} sites are reduced to highly uncoordinated Cr^{II} sites very much similar to those obtained upon pre-reduction in CO (Fig. 6c), in good agreement with the observation of a brilliant flash of light when the sample is exposed to air. These sites are accessible by CO, and take part to ethylene polymerization. However, the majority of the Cr^{VI} sites (ca. 44%) are reduced to Cr^{IV}(=O) species (Fig. 6a), i.e. chromyl mono-oxo sites, which are accessible to incoming molecules and by far more reactive than the Cr^{II} sites in ethylene polymerization, as previously demonstrated by some of us [34], [73]. Hence, the higher activity of a Cr/SiO_2 Phillips catalyst pre-reduced in CH_4 can be explained in terms of formation of a substantial amount of "super-active" Cr^{IV}(=O) species.

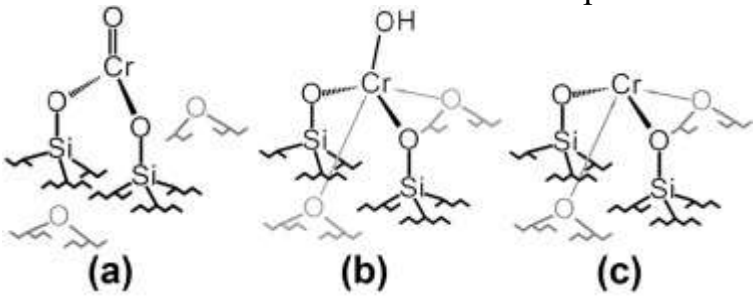

Fig. 6. Pictorial representation of the local structures for the reduced Cr-species on CH_4-Cr/SiO_2 catalyst, as suggested by spectroscopic methods.

References

1. T.E. Nowlin**Business and Technology of the Global Polyethylene Industry** Wiley-Scrivener, New York (2014)
2. H.A. Wittcoff, B.G. Reuben, J.S. Plotkin**Industrial Organic Chemicals** (third ed.), John Wiley and Sons (2013)
3. Market Report: Global Catalyst Market. Acmite Market Intelligence, Ratingen, Germany, 2015.
4. J. Jansz, Global PO&E News Analysis, Chemical Market Resources, Inc.
   C. Copéret, A. Comas-

Vives, M.P. Conley, D.P. Estes, A. Fedorov, V. Mougel, H. Nagae, F. Núñez-Zarur, P.A. Zhizhko Chem. Rev., 116 (2016), pp. 323-421
5. H.R. Sailors, J.P. Hogan J. Macromol. Sci. Pure Appl. Chem., 15 (1981), pp. 1377-1402
6. T.J. Hutley, M. Ouederni, in: M.A.-A. AlMa'adeed, I. Krupa, (Eds.), Polyolefin Compounds and materials, Springer, Switzerland, pp. 13–50.
7. W. Kaminsky Macromolecules, 45 (2012), pp. 3289-3297
8. W. Kaminsky Rend. Fis. Acc. Lincei, 28 (2017), pp. 87-95
9. D. Cicmil, J. Meeuwissen, A. Vantomme, J. Wang, I.K. Van Ravenhorst, H.E. Van Der Bij, A. Muñoz-Murillo, B.M. Weckhuysen Angew. Chem. Int. Ed., 54 (2015), pp. 13073-13079
10. M.P. McDaniel Adv. Catal., 53 (2010), pp. 123-606
11. M. McDaniel MRS Bull., 38 (2013), pp. 234-238
12. M.P. McDaniel, in: G. Ertl, H. Knözinger, and J. Weitkamp, (Eds.), Handbook of heterogeneous catalysis, VHC, Weinheim. 2400.
13. Zecchina, E. Garrone, G. Ghiotti, C. Morterra, E. Borello J. Phys. Chem., 79 (1975), pp. 966-972
14. Fubini, G. Ghiotti, L. Stradella, E. Garrone, C. Morterra J. Catal., 66 (1980), pp. 200-213
15. B.M. Weckhuysen, I.E. Wachs J. Chem. Soc. Faraday Trans., 92 (1996), pp. 1969-1973
16. B.M. Weckhuysen, I.E. Wachs, R.A. Shoonheydt Chem. Rev., 96 (1996), pp. 3327-3349
17. E. Groppo, C. Lamberti, S. Bordiga, G. Spoto, A. Zecchina Chem. Rev., 105 (2005), pp. 115-184
18. R. Cheng, Z. Liu, L. Zhong, X. He, P. Qiu, M. Terano, M.S. Eisen, S.L. Scott, and B. Liu, in: W. Kaminsky, (Ed.), Polyolefins: 50 years after Ziegler and Natta I, Springer Berlin Heidelberg, Berlin, Heidelberg. 135-202.
19. M.P. McDaniel J. Catal., 261 (2009), pp. 34-49
20. B. Liu, H. Nakatani, M. Terano J. Mol. Catal. A: Chem., 184 (2002), pp. 387-398
21. L. Zhong, Z. Liu, R. Cheng, S. Tang, P. Qiu, X. He, M. Terano, B. Liu ChemCatChem, 4 (2012), pp. 872-881
22. C. Barzan, A. Piovano, L. Braglia, G.A. Martino, C. Lamberti, S. Bordiga, E. Groppo J. Am. Chem. Soc., 139 (2017), pp. 17064-17073
23. D. Stoiljković, B. Pilić, M. Bulajić, N. Durasović, N. Ostrovski J. Serb. Chem. Soc., 72 (2007), pp. 1155-1169
24. K.C. Potter, C.W. Beckerle, F.C. Jentoft, E. Schwerdtfeger, M.P. McDaniel J. Catal., 344 (2016), pp. 657-668
25. E. Morra, G.A. Martino, A. Piovano, C. Barzan, E. Groppo, M. Chiesa J. Phys. Chem. C, 122 (2018), pp. 21531-21536
26. E. Groppo, G.A. Martino, A. Piovano, C. Barzan ACS Catal., 8 (2018), pp. 10846-10863
27. J.N. Finch J. Catal., 43 (1976), pp. 111-121
28. J.P. Hogan, D.R. Witt Am. Chem. Soc. Div. Pet. Chem. Prepr., 24 (1979)
29. L.K. Przhevalskaya, V.A. Shvets, V.B. Kazansky J. Catal., 39 (1975), pp. 363-368
30. B. Rebenstorf Acta Chem. Scand. A, 43 (1989), p. 413
31. B. Rebenstorf J. Mol. Catal., 56 (1989), pp. 170-182
32. B. Rebenstorf J. Mol. Catal., 66 (1991), pp. 59-71
33. E. Groppo, A. Damin, C. Otero Arean, A. Zecchina Chem. Eur. J., 17 (2011), pp. 11110-11114
34. C. Barzan, A.A. Damin, A. Budnyk, A. Zecchina, S. Bordiga, E. Groppo J. Catal., 337 (2016), pp. 45-51
35. L. Li, Y. Wu, Q. Dong, A. Hao, R. Cheng, L. Zhong, B. Liu Asia-Pac. J. Chem. Eng., 8 (2013), pp. 539-546
36. Y. Zeng, P. Chammingkwan, R. Baba, T. Taniike, M.C. Terano Macromol. React. Eng., 11 (2017)

37. H.L. Krauss, H. Stach Inorg. Nucl. Chem. Lett., 4 (1968), pp. 393-397
38. Zecchina, E. Garrone, G. Ghiotti, S. Coluccia J. Phys. Chem., 79 (1975), pp. 972-978
39. Bensalem, B.M. Weckhuysen, R.A. Schoonheydt J. Phys. Chem. B, 101 (1997), pp. 2824-2829
40. Brown, J. Krzystek, R. Achey, A. Lita, R. Fu, R.W. Meulenberg, M. Polinski, N. Peek, Y. Wang, L.J. Van De Burgt, S. Profeta, A.E. Stiegman, S.L. Scott ACS Catal., 5 (2015), pp. 5574-5583
41. Groppo, K. Seenivasan, C. Barzan **Catal** Sci. Technol., 3 (2013), pp. 858-878
42. Brown, A. Lita, Y. Tao, N. Peek, M. Crosswhite, M. Mileham, J. Krzystek, R. Achey, R. Fu, J.K. Bindra, M. Polinski, Y. Wang, L.J. Van De Burgt, D. Jeffcoat, S. Profeta, A.E. Stiegman, S.L. Scott ACS Catal., 7 (2017), pp. 7442-7455
43. P. Morys, U. Gorges, H.L. Krauss, Z. Naturforsh B: Anorg. Chem., Org. Chem., 39 (1984), pp. 458-467
44. E. Groppo, C. Lamberti, G. Spoto, S. Bordiga, G. Magnacca, A. Zecchina J. Catal., 236 (2005), pp. 233-244
45. M. Lezanska, G.S. Szymanski, P. Pietrzyk, Z. Sojka, J.A. Lercher J. Phys. Chem. C, 111 (2007), pp. 1830-1839
46. Y. Wang, Y. Ohishi, T. Shishido, Q.H. Zhang, W. Yang, Q. Guo, H.L. Wan, K. Takehira J. Catal., 220 (2003), pp. 347-357
47. M. Botavina, C. Barzan, A. Piovano, L. Braglia, G. Agostini, G. Martra, E. Groppo Catal. Sci. Technol., 7 (2017), pp. 1690-1700
48. O. Mathon, A. Beteva, J. Borrel, D. Bugnazet, S. Gatla, R. Hino, I. Kantor, T. Mairs, M. Mu noz, S. Pasternak, F. Perrin, S. Pascarelli J. Synchrotron Radiat., 22 (2015), pp. 1548-1554
49. Ravel, M. Newville J. Synchrot. Radiat., 12 (2005), pp. 537-541
50. S. Krimm, C.Y. Liang, G.B.B.M. Sutherland J. Chem. Phys., 25 (1956), pp. 549-562
51. J.R. Nielsen, A.H. Woollett J. Chem. Phys., 26 (1957), pp. 1391-1401
52. Chelazzi, M. Ceppatelli, M. Santoro, R. Bini, V. Schettino Nat. Mater., 3 (2004), pp. 470-475
53. Burneau, J.-P. Gallas, in: A.P. Legrand, (Ed.), The Surface Properties of Silica, Wiley, Chichester (U.K.), p. 145−312.
54. C.A. Demmelmaier, R.E. White, J.A. van Bokhoven, S.L. Scott J. Phys. Chem. C, 112 (2008), pp. 6439-6449
55. C.A. Demmelmaier, R.E. White, J.A. van Bokhoven, S.L. Scott J. Catal., 262 (2009), pp. 44-56
56. Zecchina, S. Coluccia, E. Guglielminotti, G. Ghiotti J. Phys. Chem., 75 (1971), pp. 2774-2783
57. G. Agostini, E. Groppo, S. Bordiga, A. Zecchina, C. Prestipino, F. D'Acapito, E. van Kimmenade, P.C. Thune, J.W. Niemantsverdriet, C. Lamberti J. Phys. Chem. C, 111 (2007), pp. 16437-16444
58. B.M. Weckhuysen, R.A. Schoonheydt, J.M. Jehng, I.E. Wachs, S.J. Cho, R. Ryoo, S. Kijlstr a, E. Poels J. Chem. Soc. Faraday Trans., 91 (1995), pp. 3245-3253
59. C. Pak, G.L. Haller Micropor. Mesopor. Mat., 48 (2001), pp. 165-170
60. Groppo, C. Prestipino, F. Cesano, F. Bonino, S. Bordiga, C. Lamberti, P.C. Thüne, J.W. Nie mantsverdriet, A. Zecchina J. Catal., 230 (2005), pp. 98-108
61. M. Tromp, J.O. Moulin, G. Reid, J. Evans, A.I.P. Conf Proc., 882 (2007), pp. 699-701
62. Zecchina, C.O. Arean, E. Groppo ChemCatChem, 2 (2010), pp. 259-262
63. D. Gianolio, E. Groppo, J.G. Vitillo, A. Damin, S. Bordiga, A. Zecchina, C. Lamberti Chem. Commun., 46 (2010), pp. 976-978
64. B.N. Figgis**Introduction to Ligand Fields** John Wiley & Sons, New York (1966)

65. B.M. Weckhuysen, L.M. Deridder, R.A. Schoonheydt J. Phys. Chem., 97 (1993), pp. 4756-4763
66. B.M. Weckhuysen, A.A. Verberckmoes, A.L. Buttiens, R.A. Schoonheydt J. Phys. Chem., 98 (1994), pp. 579-584
67. A.T. Casey, J.H. Clark Inorg. Chem., 7 (1968), pp. 1598-1602
68. A.A. Guda, S.A. Guda, K.A. Lomachenko, M.A. Soldatov, I.A. Pankin, A.V. Soldatov, L. B raglia, A.L. Bugaev, A. Martini, M. Signorile, E. Groppo, A. Piovano, E. Borfecchia, C. La mberti Catal. Today (2019)
69. C. Lamberti, A. Zecchina, E. Groppo, S. Bordiga Chem. Soc. Rev., 39 (2010), pp. 4951-5001
70. Ghiotti, E. Garrone, A. Zecchina J. Mol. Catal., 46 (1988), pp. 61-77
71. A.B. Gaspar, J.L.F. Brito, L.C. Dieguez J. Mol. Catal. A, 203 (2003), pp. 251-266
72. E. Groppo, A. Zecchina, C. Barzan, J.G. Vitillo Phys. Chem. Chem. Phys., 14 (2012), pp. 6538-6543
73. Zecchina, E. Groppo Proc. R. Soc. A-Math. Phys. Eng. Sci., 468 (2012), pp. 2087-2098
74. S.D. Kohler, J.G. Ekerdt J. Phys. Chem., 98 (1994), pp. 4336-4342
75. E. Groppo, C. Lamberti, F. Cesano, A. Zecchina Phys. Chem. Chem. Phys., 8 (2006), pp. 2453-2456
76. T.F. McKenna, V. Mattioli Macromol. Symp., 173 (2001), pp. 149-162
77. N.M. Ostrovskii, D. Stoiljković Theor. Found. Chem. Eng., 45 (2011), pp. 40-52
78. G.A. Martino, C. Barzan, A. Piovano, A. Budnyk, E. Groppo J. Catal., 357 (2018), pp. 206-212